IOPscience iopscience.iop.org

Home Search Collections Journals About Contact us My IOPscience

Investigating electron depletion effect in amorphous indium–gallium–zinc-oxide thin-film transistor with a floating capping metal by technology computer-aided design simulation and leakage reduction

This content has been downloaded from IOPscience. Please scroll down to see the full text.

2014 Jpn. J. Appl. Phys. 53 064302

(http://iopscience.iop.org/1347-4065/53/6/064302)

View the table of contents for this issue, or go to the journal homepage for more

Download details:

IP Address: 140.113.38.11
This content was downloaded on 25/12/2014 at 03:09

Please note that terms and conditions apply.

Japanese Journal of Applied Physics **53**, 064302 (2014)
http://dx.doi.org/10.7567/JJAP.53.064302

REGULAR PAPER

Investigating electron depletion effect in amorphous indium–gallium–zinc-oxide thin-film transistor with a floating capping metal by technology computer-aided design simulation and leakage reduction

Ting-Chou Lu[1], Wei-Tsung Chen[2], Hsiao-Wen Zan[2*], and Ming-Dou Ker[1]

[1]*Nanoelectronics and Gigascale Systems Laboratory, Institute of Electronics, National Chiao Tung University, Hsinchu 300, Taiwan*
[2]*Department of Photonics and Institute of Electro-Optical Engineering, National Chiao Tung University, Hsinchu 300, Taiwan*
E-mail: hsiaowen@mail.nctu.edu.tw

Received September 14, 2013; accepted March 11, 2014; published online May 15, 2014

The electron distribution in an amorphous indium–gallium–zinc-oxide (a-IGZO) thin-film transistor (TFT) with a floating metal–semiconductor (MS) back interface is analyzed using a technology computer-aided design (TCAD) model. The channel geometry (i.e., length and thickness) effect is carefully investigated. At a high work function (i.e., 5 eV) of the capping metal, electrons inside a-IGZO are mostly removed by the capping metal (electron depletion effect). The depletion of the IGZO film leads to an increase in threshold voltage in a-IGZO TFT. TCAD simulation reveals that increasing channel length and decreasing IGZO thickness significantly enhance such an electron depletion effect. Finally, the electron depletion effect is applied to a-IGZO TFT with a high-conductivity IGZO film to greatly suppress the leakage current by over 5 orders.
© 2014 The Japan Society of Applied Physics

1. Introduction

Recently, amorphous indium–gallium–zinc-oxide (a-IGZO) thin-film transistors (TFTs) have attracted considerable interest for applications in the active-matrix (AM) backplane of liquid-crystal displays (LCDs) and organic light-emitting diode (OLED) displays[1–4] because of their excellent characteristics, such as high mobility and uniform amorphous structure.[5–9] Electron transport in a-IGZO is known to follow percolation transport.[10–13] Potential barriers generated owing to the random distribution of Ga^{3+} and Zn^{2+} ions in the network structure strongly limit the carrier transport. Increasing carrier concentration can reduce the potential barrier and hence improve carrier mobility.[8,14–17] A high electron concentration in the channel region, however, leads to either leakage between the source and drain electrodes or a negatively shift threshold voltage.[18] To achieve a better control of leakage current, the electron concentration should be kept low in the channel region.[19–21] Even with an identical IGZO film property, capping different materials onto the back interface of a-IGZO may also affect the carrier concentration in the channel region.[22,23] In our previous work, we investigated the threshold voltage shift in a-IGZO TFT by capping a floating metal onto the back interface of a-IGZO.[24] Electron depletion or electron injection was proposed to explain the threshold voltage shift when the capping metal has a high work function (e.g., 5 eV) or a low work function (2.9 eV), respectively.[25] Here, by Silvaco technology computer-aided design (TCAD) simulation, we further investigate the geometry effect of the electron depletion phenomenon.[26–30] Two-dimensional electron distribution reveals that capping floating metal with a high work function (e.g., 5 eV) reduces channel electron concentration from 8×10^{16} to 1×10^{11} cm^{-3}. Reducing film thickness and increasing channel length enhances the electron depletion effect. Finally, we applied the electron depletion effect in our leakage control experiment. For a-IGZO TFT with a UV-treated conductive channel, capping a floating gold onto the central region of the back interface reduces the off-state current from 3×10^{-4} to 5×10^{-9} A.

2. Simulation setting

The insets of Figs. 1(a) and 1(b) show the schematic diagrams of a standard bottom gate a-IGZO TFT (STD device) and a floating-metal-capped (FMC) IGZO TFT. In this study, the source and drain electrodes are 10-nm-thick titanium (Ti). The gate insulator is a 100-nm-thick silicon nitride. The channel length is in the range from 200 to 2 µm. The IGZO thickness is changed from 50 to 10 nm. For FMC IGZO TFT, a floating metal with a work function ranging from 5.5 to 4 eV is capped onto the central region of the back interface between the source and the drain electrodes. The length of the floating metal is fixed at one-half of the channel length. To examine electron distribution under thermal equilibrium, the drain-to-source voltage (V_{DS}) and gate-to-source voltage (V_{GS}) are both 0 V. The permittivity, electron affinity, and energy gap at 300 K of IGZO are 4 F/m, 3.8 eV, and 3 eV, respectively. The defects in the IGZO film including the tail state as well as deep level are considered in the device simulations.[30,31] The parameters that determine the density of state (DOS) distribution of IGZO are given in Ref. 32. The electron and hole mobility are 10 and 10^{-5} cm^2 V^{-1} s^{-1}, respectively. Different gate biases are applied only in Figs. 3(a) and 4(c) when we discuss the restoring of electron concentration.

3. Experimental methods

Heavily doped p-type Si(100) was used as a substrate and a gate electrode. A 100-nm-thick silicon nitride layer was deposited by low pressure chemical vapor deposition at 780 °C to serve as the gate dielectric. Then, a 35-nm-thick a-IGZO layer (3 in. circular target, In : Ga : Zn = 1 : 1 : 1 at%) was deposited through a shadow mask at room temperature using a radio-frequency sputtering system with a power of 100 W, a working pressure of 5 mTorr, and an Ar flow rate of 20 sccm. The width of the IGZO layer is used to define the channel width (W) as 1000 µm. Then, 100-nm-thick Ti pads were evaporated through a shadow mask to form the source and drain electrodes and to define the channel length (L) as 400 µm. UV treatment was carried out in nitrogen environ-

© 2014 The Japan Society of Applied Physics

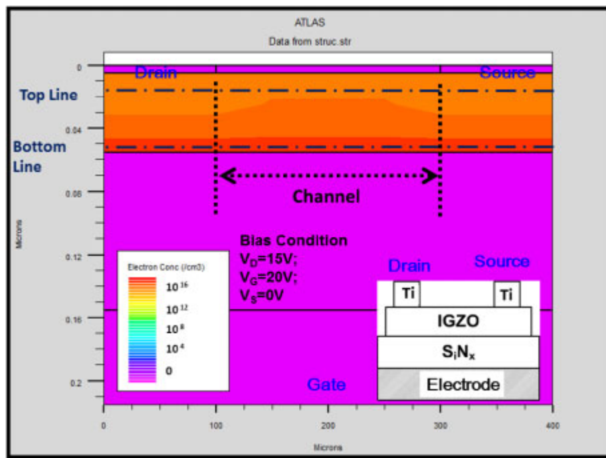

(a)

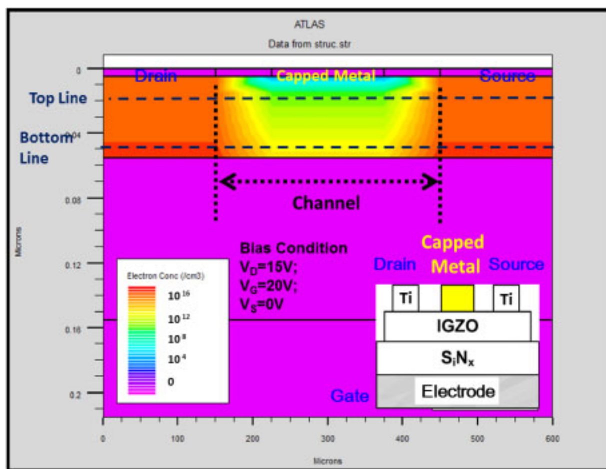

(b)

Fig. 1. (Color online) Two-dimensional electron concentration for (a) a standard (STD) a-IGZO TFT and (b) a FMC IGZO TFT. The work function of the floating metal in (b) is 5 eV.

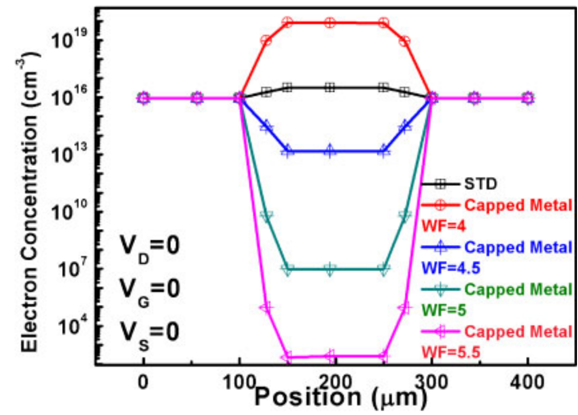

(a)

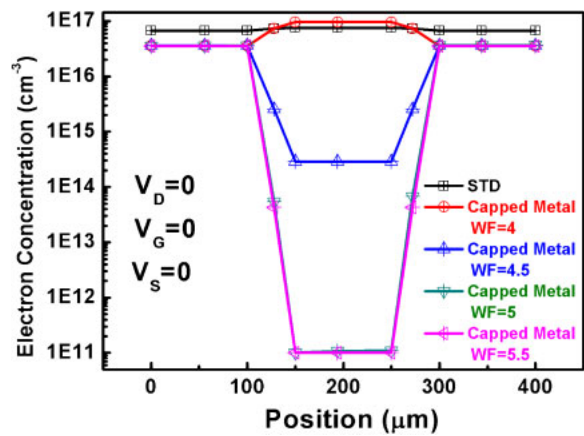

(b)

Fig. 2. (Color online) Electron concentration along (a) *Top Line* and (b) *Bottom Line* in STD and FMC IGZO TFTs with different work functions of the floating metal.

ment at a wavelength of 172 nm and a power density of 50 mW/cm^2 using a Xe excimer lamp. Finally, the gold pad (width 1000 µm; length 200 µm) was evaporated through a shadow mask to cap the central region of the back interface. All electrical characteristics were measured by using an Agilent 4156 current–voltage analyzer. The threshold voltage and mobility were extracted from the slope and the x-axis intercept of the $\sqrt{I_D}$–V_G curves in the saturation region ($V_D = 20$ V).

4. Simulation results

Firstly, we compare the two-dimensional electron distribution in a standard IGZO TFT and a FMC IGZO TFT, as shown in Figs. 1(a) and 1(b), respectively. In Figs. 1(a) and 1(b), the channel length is 200 µm and the IGZO thickness is 50 nm. The work function of the floating metal is 5 eV. We can clearly observe that the electron concentration under the floating metal in Fig. 1(b) is much lower than that in the central channel region of the STD device in Fig. 1(a). We further compare the electron concentration close to the back interface and front channel by plotting the one-dimensional electron distribution along the Top Line and Bottom Line, respectively. The Top Line, as shown in Figs. 1(a) and 1(b), locates in the upper IGZO film with a distance from the back interface corresponding to 10% IGZO thickness. The Bottom Line, on the other hand, locates in the lower IGZO film with a distance from the front interface corresponding to 10% IGZO thickness.

Figure 2(a) shows the electron concentration along the Top Lines when the floating capping metal exhibits different work functions. The ratio of channel length to capping metal length is kept at 2 : 1. The work function of the capping metal varies from 4 to 5.5 eV. As the work function of the capping metal increases, the electron concentration in the channel decreases. The IGZO body is almost depleted when the work function of the capping metal is 5.5 eV. This verifies that electrons in IGZO are removed by the capping metal when the work function of the capping metal is higher than that of IGZO. When the work function of the capping metal is 4, the electron concentration is higher than that of the STD device, revealing the injection of electrons from the capping metal to the IGZO film.

The electron concentrations along the Bottom Lines when the floating capping metal exhibits different work functions are shown in Fig. 2(b). When the the work function of the capping metal is, 4.5, 5, or 5.5 eV, the electron concentration at the Bottom Line is significantly reduced, indicating that the electron depletion effect also affects the electron concen-

 © 2014 The Japan Society of Applied Physics

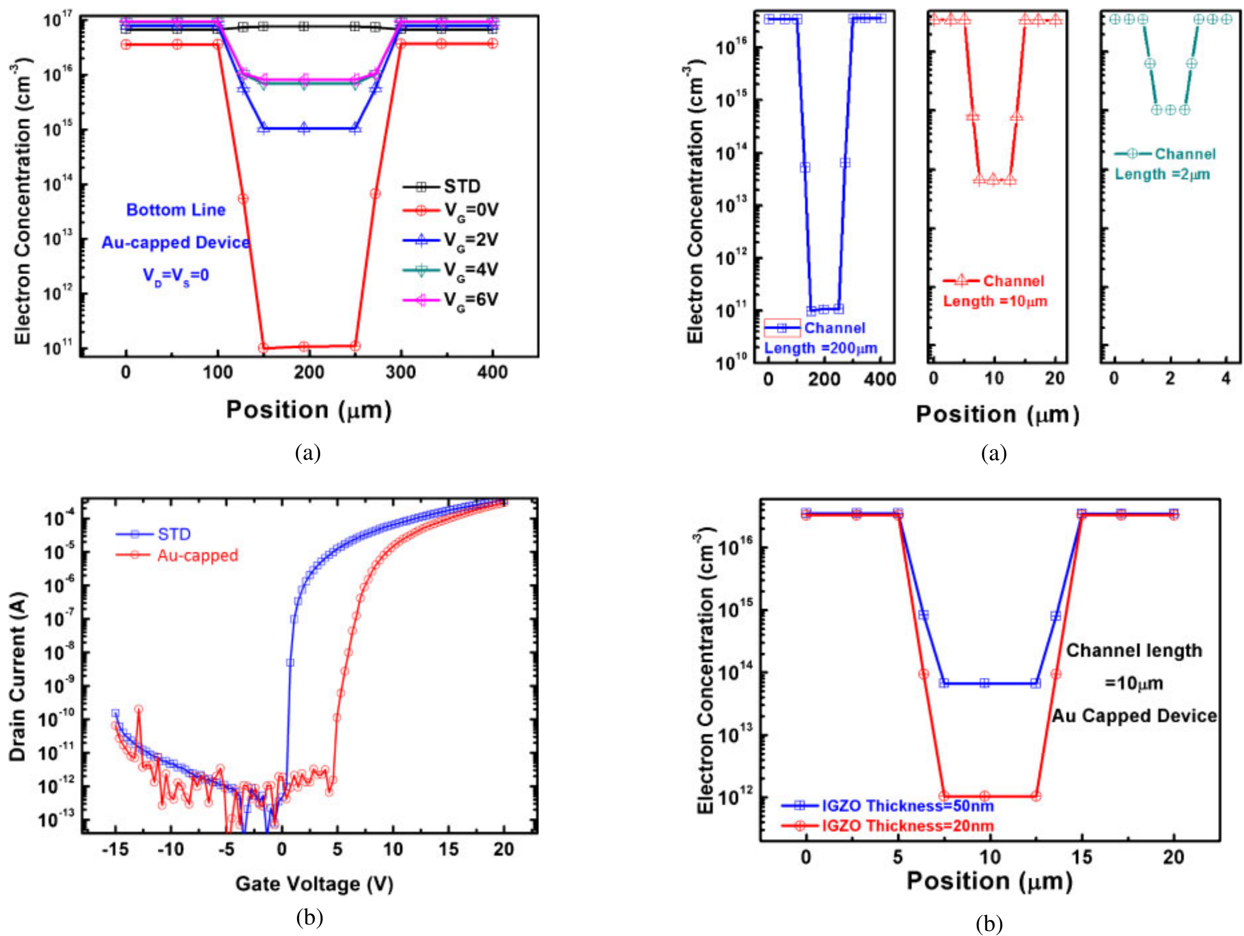

Fig. 3. (Color online) (a) Electron concentration of STD and FMC a-IGZO TFT with different gate biases. The drain and source are grounded ($V_D = V_S = 0$). (b) Experimental transfer characteristics of STD and Au-capped a-IGZO TFTs.

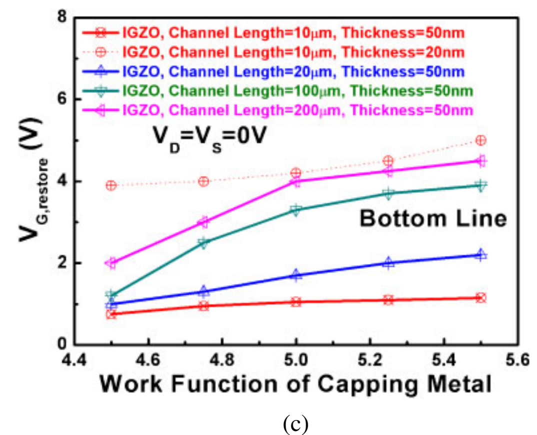

Fig. 4. (Color online) *Bottom-Line* electron concentrations of Au-capped IGZO TFT with (a) different channel lengths and (b) different IGZO thicknesses. (c) $V_{G,restore}$ plotted as the work function of the floating capping metal with different channel lengths and IGZO thicknesses.

tration in the front channel region. A more positive threshold voltage is required to induce sufficient electrons in front channel to turn on the transistor. For such electron-depleted devices, the influences of gate bias on electron concentration at the Bottom Line are investigated. As shown in Fig. 3(a), for the Au-capped device (i.e., for a work function of 5 eV), the electron concentration at central position increases from 1×10^{11} to $9 \times 10^{15}\,\mathrm{cm}^{-3}$ when the gate bias is increased from 0 to 6 V. For the STD device, the front-channel electron concentration is $8.5 \times 10^{16}\,\mathrm{cm}^{-3}$. The results shown in Fig. 3(a) suggest that, by applying a suitable gate bias, the electron concentration at the Bottom Line of FMC IGZO TFT can be almost identical to that of STD IGZO TFT. The applied gate bias, which restores the electron concentration of FMC IGZO TFT, is about 6 V. Experimentally, as shown in Ref. 19 and reproduced in Fig. 3(b), a 6 V threshold voltage shift is also observed when the capping the floating gold metal onto the back interface of a-IGZO TFT. It is noted that the device geometry in experimental results [Fig. 3(b)] and that in simulated results [Fig. 3(a)] are the same. Here, we define that the gate bias applied to restore the Bottom-Line electron concentration is named $V_{G,restore}$.

We then further compare the *Bottom-Line* electron concentrations of Au-capped IGZO TFT with different channel lengths and different IGZO thicknesses in Figs. 4(a) and 4(b), respectively. When the channel length is reduced from 200 to 10, and 2 μm as shown in Fig. 4(a), the electron depletion effect is suppressed. With a fixed channel length as 10 μm, in Fig. 4(b), electron depletion effect becomes more significant when IGZO thickness decreases from 50 to 20 nm, as shown in Fig. 4(b). The geometry effect can be observed more clearly when comparing $V_{G,restore}$ of devices with different channel geometries and with different capping metals. In Fig. 4(c), $V_{G,restore}$ is plotted as the work function of the floating capping metal. For all these cases with different channel lengths and different IGZO thicknesses, $V_{G,restore}$

© 2014 The Japan Society of Applied Physics

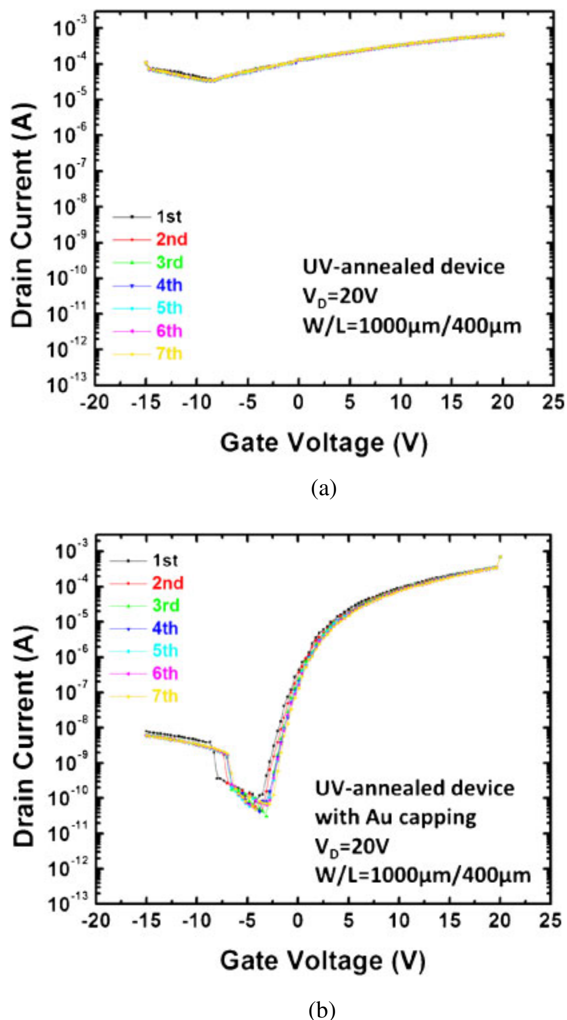

Fig. 5. (Color online) Experimental transfer characteristics of (a) UV-annealed a-IGZO TFT and (b) UV-annealed a-IGZO TFT after Au capping. Continuous measurements 7 times are shown.

becomes more positive when the work function of the capping metal is increased. Reducing channel length and increasing IGZO thickness lead to a reduction in $V_{G,restore}$. Specifically speaking, for a channel length of 10 μm and an IGZO thickness of 50 nm, $V_{G,restore}$ is lower than 1.2 V, indicating that the capping metal has only a negligible influence on device performance. Reducing the IGZO thickness to 20 nm and keeping the channel length at 10 μm, however, produce a high $V_{G,restore}$ (3.5 to 5 V) owing to the electron depletion effect.

Finally, experimentally, we demonstrate the leakage reduction effect by utilizing the electron depletion due to gold capping. The transfer characteristics of the initial a-IGZO TFT after UV annealing are shown in Fig. 5(a). A high concentration of oxygen deficiency is produced following UV exposure. Hence, the carrier concentration in the IGZO film is increased to generate a high leakage current (3×10^{-4} A) between the source and drain electrodes. After capping the gold metal onto the central region of the back interface, the transfer characteristics of Au-capped IGZO TFT are shown in Fig. 5(b). Good transistor performance can be obtained and the leakage current is reduced to be 5×10^{-9} A. The extracted mobility, threshold voltage, subthreshold swing, and on/off current ratio are 15 $cm^2 V^{-1} s^{-1}$, 1.4 V, 0.72 V/dec, and 5×10^6, respectively.

5. Conclusions

In this study, the two-dimensional electron distribution of n-channel a-IGZO TFT with a floating metal–semiconductor (MS) back contact is demonstrated using a Silvaco TCAD simulator. The simulated results verify that capping metals with various work functions on the IGZO back interface significantly affects electron distribution. In particular, when capping a floating metal with a high work function, electrons inside the IGZO film are obviously depleted. The electron depletion effect can also affect the electron concentration in the front channel region and hence lead to a shift of threshold voltage. Increasing channel length and reducing IGZO film thickness effectively enhance the electron depletion effect. Finally, experimentally, the electron depletion effect is used to reduce leakage current. For UV-treated a-IGZO TFT with an initially conductive channel, capping a floating gold metal onto the IGZO back interface effectively lower decreases the off-state current from 3×10^{-4} to 5×10^{-9} A.

Acknowledgement

The authors thank Ministry of Science and Technology in Taiwan for financial support under grant number 101-2221-E-009-051-MY2.

1) J.-H. Lee, D.-H. Kim, D.-J. Yang, S.-Y. Hong, K.-S. Yoon, P.-S. Hong, C.-O. Jeong, H.-S. Park, S. Y. Kim, S. K. Lim, S. S. Kim, K.-S. Son, T.-S. Kim, J.-Y. Kwon, and S.-Y. Lee, SID Symp. Dig. Tech. Pap. **39**, 625 (2008).
2) J. K. Jeong, J. H. Jeong, J. H. Choi, J. S. Im, S. H. Kim, H. W. Yang, K. N. Kang, K. S. Kim, T. K. Ahn, H.-J. Chung, M. Kim, B. S. Gu, J.-S. Park, Y.-G. Mo, H. D. Kim, and H. K. Chung, SID Symp. Dig. Tech. Pap. **39**, 1 (2008).
3) T.-C. Fung, C.-S. Chuang, K. Nomura, H.-P. D. Shieh, H. Hosono, and J. Kanicki, J. Inf. Disp. **9** [4], 21 (2008).
4) T.-C. Fung, C.-S. Chuang, B. G. Mullins, K. Nomura, T. Kamiya, H.-P. D. Shieh, H. Hosono, and J. Kanicki, 32nd Int. Meet. Information of Display, 2008, p. 1208.
5) S. Jeon, S. Park, I. Song, J.-H. Hur, J. Park, S. Kim, S. Kim, H. Yin, E. Lee, S. Ahn, H. Kim, H. Kim, C. Kim, and U. Chung, IEDM Tech. Dig., 2010, 21.3.1.
6) B. Kim, S. C. Choi, J.-S. Lee, S.-J. Kim, Y.-H. Jang, S.-Y. Yoon, C.-D. Kim, and M.-K. Han, IEEE Trans. Electron Devices **58**, 3012 (2011).
7) H. Hosono, M. Yasukawa, and H. Kawazoe, J. Non-Cryst. Solids **203**, 334 (1996).
8) H. Hosono, J. Non-Cryst. Solids **352**, 851 (2006).
9) A. Takagi, K. Nomura, H. Ohta, H. Yanagi, T. Kamiya, M. Hirano, and H. Hosono, Thin Solid Films **486**, 38 (2005).
10) K. Nomura, H. Ohta, A. Takagi, T. Kamiya, M. Hirano, and H. Hosono, Nature **432**, 488 (2004).
11) P. Bhattacharya, *Semiconductor Optoelectronic Devices* (Prentice Hall, Upper Saddle River, NJ, 1997) p. 87.
12) G. Fortunato, L. Mariucci, and C. Reita, *Amorphous and Microcrystalline Semiconductor Devices-Materials and Device Physics* (Artech House, Norwood, MA, 1992) p. 132.
13) E. M. C. Fortunato, P. M. C. Barquinha, A. C. M. B. G. Pimentel, A. M. F. Gonçalves, A. J. S. Marques, R. F. P. Martins, and L. M. N. Pereira, Appl. Phys. Lett. **85**, 2541 (2004).
14) W. Jackson, R. Hoffman, and G. Herman, Appl. Phys. Lett. **87**, 193503 (2005).
15) H. Chiang, J. Wager, R. Hoffman, J. Jeong, and D. Keszler, Appl. Phys. Lett. **86**, 013503 (2005).
16) K. Nomura, H. Ohta, K. Ueda, T. Kamiya, M. Hirano, and H. Hosono, Science **300**, 1269 (2003).
17) K. Abe, N. Kaji, H. Kumomi, K. Nomura, T. Kamiya, M. Hirano, and H. Hosono, IEEE Trans. Electron Devices **58**, 3463 (2011).
18) K. Roy, S. Mukhopadhyay, and H.-M. Chen, Proc. IEEE **91**, 305 (2003).

© 2014 The Japan Society of Applied Physics

19) M. Kim, J.-H. Jeong, H.-J. Lee, T.-K. Ahn, H. S. Shin, J.-S. Park, J.-K. Jeong, Y.-G. Mo, and H.-D. Kim, Appl. Phys. Lett. **90**, 212114 (2007).
20) H. W. Zan, W. T. Chen, H. W. Hsueh, S. C. Kao, M. C. Ku, C. C. Tsai, and H. F. Meng, Appl. Phys. Lett. **97**, 203506 (2010).
21) J. M. Lee, I. T. Cho, J.-H. Lee, and H. I. Kwon, Jpn. J. Appl. Phys. **48**, 100202 (2009).
22) H. Lim, H. Yin, J.-S. Park, I. Song, C. Kim, J. Park, S. Kim, S.-W. Kim, C.-B. Lee, Y. Kim, Y. Park, and D. Kang, Appl. Phys. Lett. **93**, 063505 (2008).
23) K. Takechi, M. Nakata, K. Azuma, H. Yamaguchi, and S. Kaneko, IEEE Trans. Electron Devices **56**, 2027 (2009).
24) H.-W. Zan, W.-T. Chen, C.-C. Yen, H.-W. Hsueh, and C.-C. Tsai, Appl. Phys. Lett. **98**, 153506 (2011).
25) H. Kawazoe, M. Yasukawa, H. Hyodo, M. Kurita, H. Yanagi, and H. Hosono, Nature **389**, 939 (1997).
26) H.-H. Hsieh, T. Kamiya, K. Nomura, H. Hosono, and C.-C. Wu, Appl. Phys. Lett. **92**, 133503 (2008).
27) K. Jeon, C. Kim, I. Song, J. Park, S. Kim, S. Kim, Y. Park, J.-H. Park, S. Lee, D. M. Kim, and D. H. Kim, Appl. Phys. Lett. **93**, 182102 (2008).
28) C.-Y. Chen and J. Kanicki, Proc. Int. AMLCD, 1995, p. 46.
29) M. Orita, H. Ohta, M. Hirano, S. Narushima, and H. Hosono, Philos. Mag. B **81**, 501 (2001).
30) T.-C. Fung, C.-S. Chuang, C. Chen, K. Abe, R. Cottle, M. Townsend, H. Kumomi, and J. Kanicki, J. Appl. Phys. **106**, 084511 (2009).
31) Y.-W. Jeon, I.-S. Hur, Y.-S. Kim, M.-K. Bae, H.-K. Jung, D.-S. Kong, W.-J. Kim, J.-H. Kim, J.-M. Jang, D.-M. Kim, and D.-H. Kim, Semicond. Sci. Technol. **11**, 153 (2011).
32) The conduction band density and valence band density at 300 K are 5×10^{18} and $5 \times 10^{18}\,\mathrm{cm^{-3}}$, respectively. The density of tail states at the conduction band is $1.55 \times 10^{20}\,\mathrm{cm^{-3}\,eV^{-1}}$, the density of tail states at the valence band is $1.55 \times 10^{20}\,\mathrm{cm^{-3}\,eV^{-1}}$, the conduction-band-tail slope is 0.013 eV, and the valence-band-tail slope is 0.12 eV.

 © 2014 The Japan Society of Applied Physics